Macromolecular and biochemical changes of G0 fission yeast nuclei

Shujun Cai†, Zhi Yang Tan†, Xin Nie, Jian Shi and Lu Gan (甘露)*

Department of Biological Sciences and Centre for BioImaging Sciences, National University of Singapore, Singapore 117543
† Equal contribution
* Correspondence: lu@anaphase.org

Abstract

Cells change their cytology in response to environmental cues and stress. Notably, large changes in nuclear architecture are accompanied by transcriptional reprogramming. When starved of nitrogen, *Schizosaccharomyces pombe* cells become rounder and they enter a quiescent "G0" state. These cells have smaller nuclei and undergo near-global transcriptional repression. Here we use electron cryotomography (cryo-ET) and cell-biology approaches to investigate the structural and biochemical changes of G0 *S. pombe* nuclei. We find that G0 cells have a denser nucleoplasm and fewer chromatin-associated multi-megadalton globular complexes (megacomplexes) than proliferating cells. These structural changes are correlated with mild histone deacetylation. Induced histone hyperacetylation in G0 results in cells that have larger nuclei and less condensed chromatin. However, these histone-hyperacetylated G0 cells still have repressed transcription, few megacomplexes, and a dense nucleoplasm. Like in budding yeast, *S. pombe* G0 nuclear phenotypes are controlled by multiple biochemical factors.

Keywords: nucleus, chromatin, transcription, quiescence, yeast, cryo-ET

Introduction

The 3-D organization of the nucleus and chromatin is important for many cellular functions including transcription, replication, and DNA repair. The basic unit of chromatin is the nucleosome, consisting of approximately 147 bp of DNA wrapped around a histone octamer[1,2]. Nucleosomes resemble ~ 10-nm wide, 6-nm thick cylinders and are the most abundant macromolecular complexes in the nucleus. Closely packed nucleosomes may limit the access of nuclear macromolecular complexes to key sequences, thereby inhibiting transcription[3,4]. Consistent with this idea, repressive nucleosome post-translational modifications (histone marks) are associated with more compact chromatin[4,5]. However, the correlations between transcription, histone marks, and macromolecular packing are poorly understood *in situ*.

The fission yeast *Schizosaccharomyces pombe* is an outstanding nuclear cell-biology model organism because the cells can be synchronized in different cell-cycle states, each with distinctive changes in chromosome condensation[6,7]. When starved of nitrogen for 24 hours, nearly all proliferating *S. pombe* cells enter a non-dividing state called G0 quiescence[8] (herein called G0). G0 cells are rounder, shorter, have smaller nuclei, and more thermotolerant than proliferating cells. Furthermore, G0 cells can survive in this nitrogen-starved state for at least one month[8,9]. These cells have only ~30% of the mRNA and ~ 20% of the rRNA content of proliferating cells[10]. G0 cells are therefore an ideal model to study the relationship between extreme transcription phenotypes and nuclear cell biology at the macromolecular level.

We recently used electron cryotomography (cryo-ET) to study *S. pombe* mitotic chromosome condensation. Our cryotomograms revealed that chromatin compaction as visualized by cryo-ET is less conspicuous than what is seen by fluorescence microscopy[11]. There is no well-defined boundary between condensed chromatin and nucleoplasm because the nucleus is crowded with macromolecular complexes. We found that prometaphase cells have fewer chromatin-associated multi-megadalton globular complexes (herein called megacomplexes) than interphase cells. Furthermore, the mitotic chromatin was less compact than what we observed in nuclear lysates, in which nucleosomes are packed into large masses. This *in situ* chromatin organization is consistent with the presence of active mitotic transcription.

Here, we use cryo-ET, fluorescence microscopy, and immunoblots to compare the nuclei of proliferating and G0 *S. pombe* cells. Our study correlates the nuclear macromolecular changes with downregulation of both chromatin and nucleolar transcription. The increased chromatin compaction in G0 is correlated with a decrease in histone acetylation. Induced histone hyperacetylation during G0 entry resulted in larger G0 nuclei, but did not affect transcriptional repression and thermotolerance. These two key G0 phenotypes therefore depend on factors other than histone acetylation and nuclear compaction.

Results

Preparation of G0 cells

To enrich for G0 *S. pombe* cells (Figure S1A), we starved proliferating wild-type cells of nitrogen by incubating them in Edinburgh Minimal Media without nitrogen (EMM−N) for 24 hours[8,9]. As controls, we used two cell types. For cryo-ET analysis, we arrested temperature-sensitive *cdc10-129* cells in G1 phase[12] because G1 and G0 cells both have a 1N nuclear DNA content and because cells enter G0 from a G1-like state[13]. Note that we could not prepare G0 cells from *cdc10-129* cells because *cdc10-129* cells transferred to EMM-N did not become rounded; G0 cells were therefore prepared from the wild-type and yFS240 strains (see Methods section). In the other experiments, we also used unsynchronized proliferating cells, which are mostly in G2, the longest cell-cycle phase[14].

Following 24 hours of nitrogen starvation, wild-type cells became rounded and had smaller nuclei (Figure S1B) as reported earlier[8]. G0 chromosomes do not appear individualized like in prometaphase-arrested *nda3-KM311* cells[7]. To characterize how

the chromatin is reorganized in G0 cells, we used cryo-ET and fluorescence microscopy. Cryo-ET is a stain- and fixation-free method that can reveal the 3-D nanoscale positions of macromolecular complexes in a life-like state[15]. To make the cell samples thin enough for cryo-ET, we cut 70- or 100-nm-thick cryosections of self-pressurized-frozen cell paste. Our cryotomograms confirm that G0 cells have undergone large-scale subcellular remodeling relative to G1 cells, consistent with earlier work on proliferating cells[8,16]. For example, G0 cells have less cytoplasm and more vacuoles (Figure S1, C and D). The contrast of the G0 nuclear densities in these defocus phase-contrast cryotomograms was so low that nuclear macromolecular complexes were difficult to see in most of these cryotomograms. Therefore, all cryo-ET data reported herein were collected with Volta phase contrast, which makes it easier to see macromolecular complexes inside cellular cryotomograms[17,18].

Transcription is repressed in every G0 cell

Previous RNA-seq measurements showed that on average, G0 cells have fewer transcripts than proliferating cells[10]. To assess the transcriptional variability between cells, we performed immunofluorescence imaging on RNA polymerase II phosphorylated on serine 2 of its large subunit carboxy-terminal domain (CTD-S2P). We chose this post-translational modification because it is a conserved marker of transcriptional elongation[19,20]. As a proxy for overall RNA polymerase levels, we also performed immunofluorescence on unmodified CTDs. We found that G0 cells had lower CTD-S2P and unmodified CTD signals than G1 cells (Figure 1, A and B). These results suggest that there are fewer transcribing RNA Polymerase II complexes and possibly fewer RNA Polymerase II complexes in every G0 cell.

To characterize bulk RNA synthesis in G0 cells, we fluorescently labeled new transcripts in the *S. pombe* strain yFS240[21]. Strains like yFS240 can use exogenous uridine and its analogs[22]. Newly synthesized RNA molecules that incorporate 5-ethynyl-uridine (5-EU) are detectable after ligation with a fluorescent dye like Alexa Fluor 488[23]. As controls, we incubated proliferating yFS240 and wild-type cells with 5-EU; yFS240 cells with both 5-EU and the transcription inhibitor phenanthroline; and yFS240 cells with uridine. All 5-EU and uridine treatments were done for 10 minutes. The chromatin was stained with 4′,6-diamidino-2-phenylindole (DAPI). Fluorescence microscopy of these control cells showed nucleus-localized Alexa Fluor 488 signal above the background only in yFS240 cells that were incubated with 5-EU without

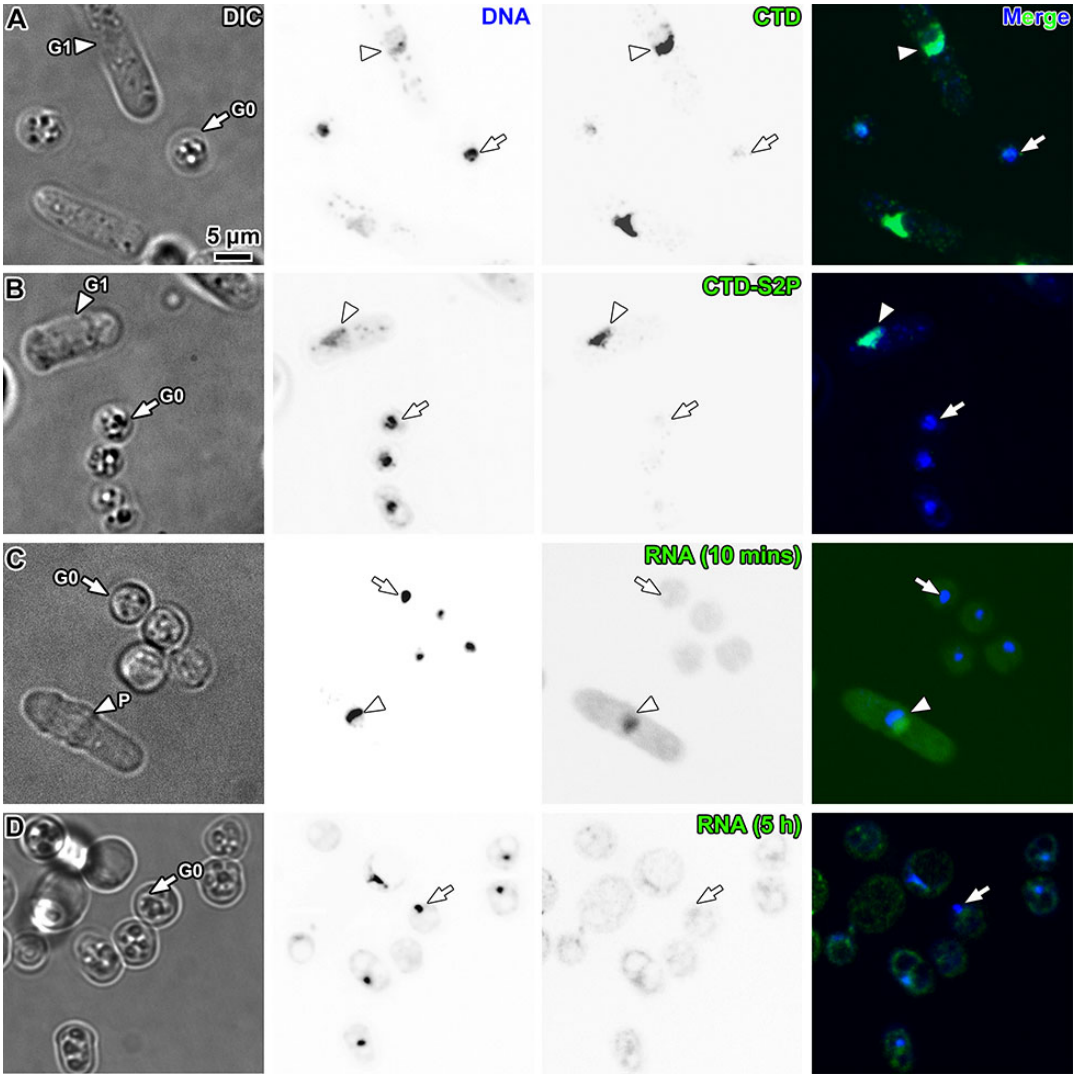

Figure 1. G0 transcription is repressed in nearly every cell. Fluorescence microscopy analysis of transcription in interphase and G0 cells. Columns, left to right: differential interference contrast (DIC), DAPI fluorescence (DNA), fluorescence (CTD, CTD-S2P, and RNA), and merge. (A) Detection of bulk RNA polymerase II with anti-yeast RNA polymerase II-CTD antibody. A G1 cell is indicated by an arrowhead and a G0 cell by an arrow. (B) Detection of elongating RNA polymerase II with the anti-CTD-S2P antibody. One G1 cell is indicated by an arrowhead and a G0 cell by an arrow. (C) Strain yFS240 G0 and proliferating (P) cells were incubated with 5-EU and subjected to the Click-iT 5-EU-detection assay, which ligates Alexa Fluor 488 to 5-EU. A proliferating cell is indicated by an arrowhead and a G0 cell by an arrow. To increase the visibility of the weak 5-EU signal, the contrast was adjusted for the entire field of view, resulting in a higher apparent background. (D) G0 cells were incubated with 5-EU for 5 hours, then subjected to Click-iT 5-EU detection as in panel C. One G0 cell is indicated by an arrow. The two larger cells in the upper left are probably dead or dying as a result of prolonged 5-EU exposure.

transcription inhibitor (Figure S2). In asynchronous proliferating cells, the newly transcribed RNA appeared more abundant in the hemisphere opposite the DAPI signal (Figure 1C). This DAPI-poor (low DNA) position corresponds to the nucleolus in *S. pombe* cells[24], meaning that the strong hemispherical 5-EU signal comes from newly synthesized rRNA (Figure 1C lower-left cell; and see the nucleolus analysis below). In comparison, 5-EU signal was much weaker in the DAPI-stained chromatin-rich half of the nucleus, where mRNA is synthesized. Such high levels of rRNA synthesis are consistent with the extremely high levels of ribosome biogenesis in yeasts[25]. In contrast to proliferating cells, G0 cells had very weak 5-EU signal (Figure 1C). To test if 10-minute incubations were too short for sufficient 5-EU-labeled RNA to accumulate in G0 cells, we increased the 5-EU incorporation to 5 hours. The 5-EU-labelled RNA signal thereafter became detectable, albeit weak, in the nucleus (Figure 1D). The 5-EU signal was also detected in the cytoplasm, possibly from the exported mRNA and ribosomes (Figure 1D). In summary, both RNA Polymerase I and Polymerase II transcription are repressed in all G0 cells.

Both G1 and G0 cells have crowded nuclei

Volta cryotomograms showed that both G1 and G0 cell nuclei are densely packed with irregularly positioned macromolecular complexes (Figure 2, A and B). Quantitative analysis of the nuclear macromolecular packing requires knowledge of the identities and positions of the nucleosome-like particles. Thus far, 3-D classification and subtomogram averaging have failed to identify yeast nucleosomes *in situ*[11]. As a compromise, we attempted 2-D classification[26] on template-matched candidate nucleosome subtomograms, which allows the elimination from consideration of false positives whose size or shape does not match

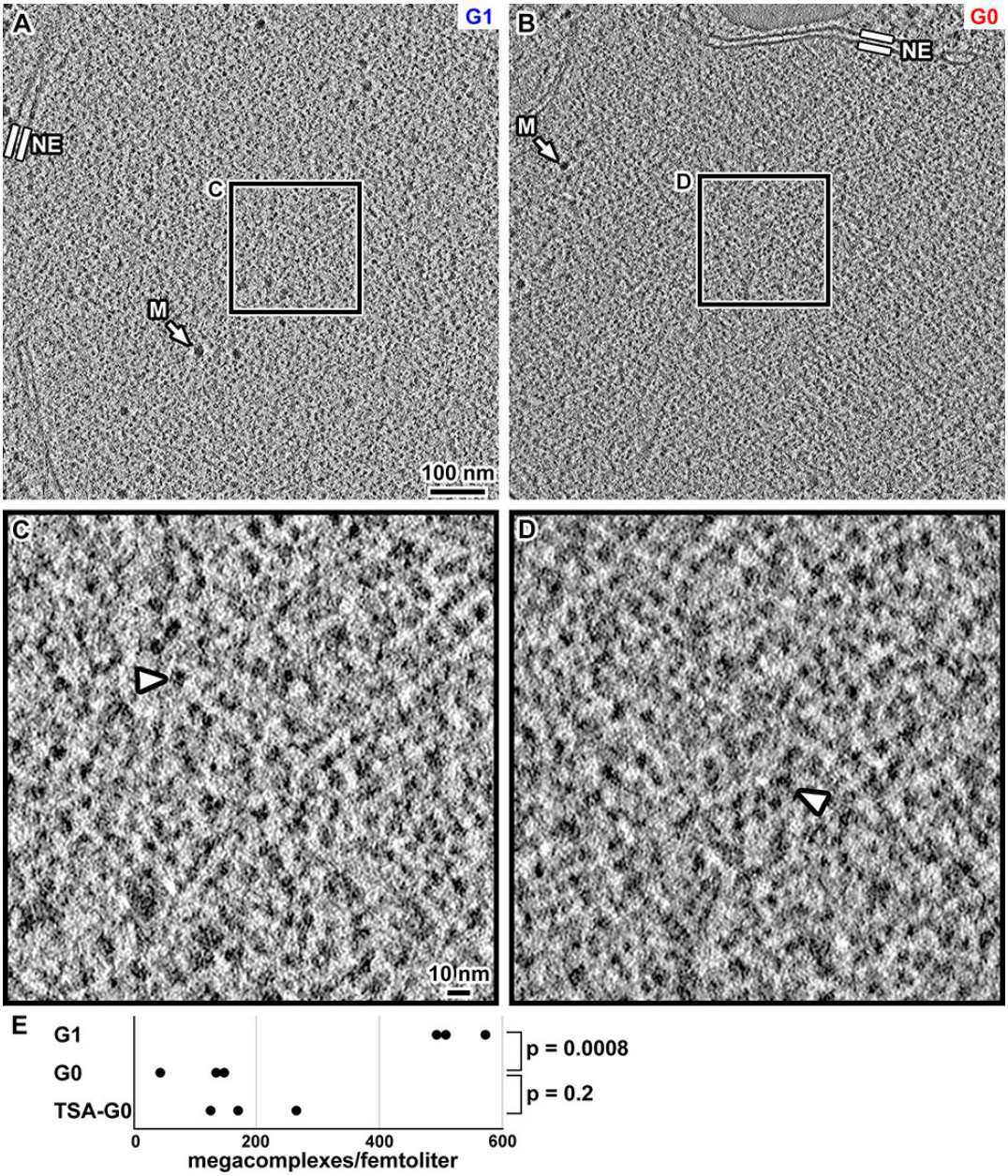

Figure 2. G0 cells have fewer megacomplexes in their nucleoplasm. (A) Volta cryotomographic 11-nm slice of the nucleus in a G1-arrested cdc10-129 cell. The nuclear envelope (NE) and a megacomplex (M) are indicated. (B) Volta cryotomographic 11-nm slice of a wild-type G0 cell, also centered on the nucleus. (C and D) Four-fold enlargements of the positions boxed in panels A and B, respectively. Nucleosome-like densities are indicated by arrowheads. (E) Quantitation of intranuclear megacomplexes from Volta cryotomograms of G1, G0 and TSA-G0 cells. The p values are from a two-tailed t-test with unequal variance, calculated using 3 technical replicates each.

nucleosomes[11]. Our 2-D classification did not adequately discriminate nucleosome-like particles because many of the class averages were ambiguous (Figure S3). This limitation could arise from the denser nucleoplasm in both G1 and G0 cells. Furthermore, the G0 nucleoplasm appears even denser than the G1 nucleoplasm (Figure 2, C and D). In both cell types, we did not find any evidence of cryo-ET densities that resemble highly compacted chromatin masses, which are present in the nuclear lysates of both budding and fission yeasts[11,27].

We previously found that *S. pombe* prometaphase cells have fewer chromatin-associated megacomplexes than G2 cells[11]. Nuclear megacomplexes include preribosomes, transcription initiation complexes, and spliceosomes, and many other globular complexes that exceed 1 megadalton molecular weight. We were unable to perform 2-D classification of megacomplexes because they were too heterogeneous. Instead, we manually annotated particles larger than ~ 15 nm. Megacomplexes were more abundant in G1 chromatin than in G0 chromatin (mean concentrations = 520 and 110 megacomplexes/femtoliter, respectively, $p = 0.0008$) (Figure 2E). We further characterized the cytology of the nucleolus, which is the most transcriptionally active nuclear compartment. Immunofluorescence images showed that G0 cells have smaller nucleoli than G1 cells (Figure 3, A and B). The smaller G0 nucleolus is consistent with previous traditional EM data[8] and with the repression of RNA polymerase I transcription. Because our cryosections sample cellular positions randomly, only a few cryosections include nucleolar densities (Figure 3, C and D). Like in G2 cells[11], megacomplexes are abundant in G1 and G0 nucleoli (Figure 3, E - H).

Prolonged G0 results in small changes to transcriptional repression

S. pombe cells that are starved of nitrogen for more than 2 weeks are still viable[8,28]. This condition, also called "deep quiescence", makes it possible to characterize potentially more extreme nuclear changes. We confirmed that cells starved of nitrogen for 20 days (herein called G0-20d) also have small nuclei (Figure S4A). Furthermore, G0-20d cells exhibit thermotolerance (Figure S4B), a G0 phenotype that is conserved in yeasts[8,29]. To determine whether RNA polymerase II transcription changes in deep-quiescent cells, we performed immunofluorescence of both unphosphorylated RNA polymerase II CTD and CTD-S2P. We detected weak unphosphorylated-CTD and CTD-S2P IF signals in G0 cells but not deep-quiescent cells (Figure S4, C and D), meaning that transcription is more repressed after prolonged quiescence.

To determine if the deep-quiescent cells undergo further nuclear cytological changes, we imaged cryosections of G0-20d cells by cryo-ET (Figure S5, A and B). G0-20d cell nuclei cryotomograms also have low contrast, meaning that their nucleoplasm is also dense like in G0. Some cells have large intranuclear aggregates (Figure S5, C and D) that we have not seen in G0 cells after 24

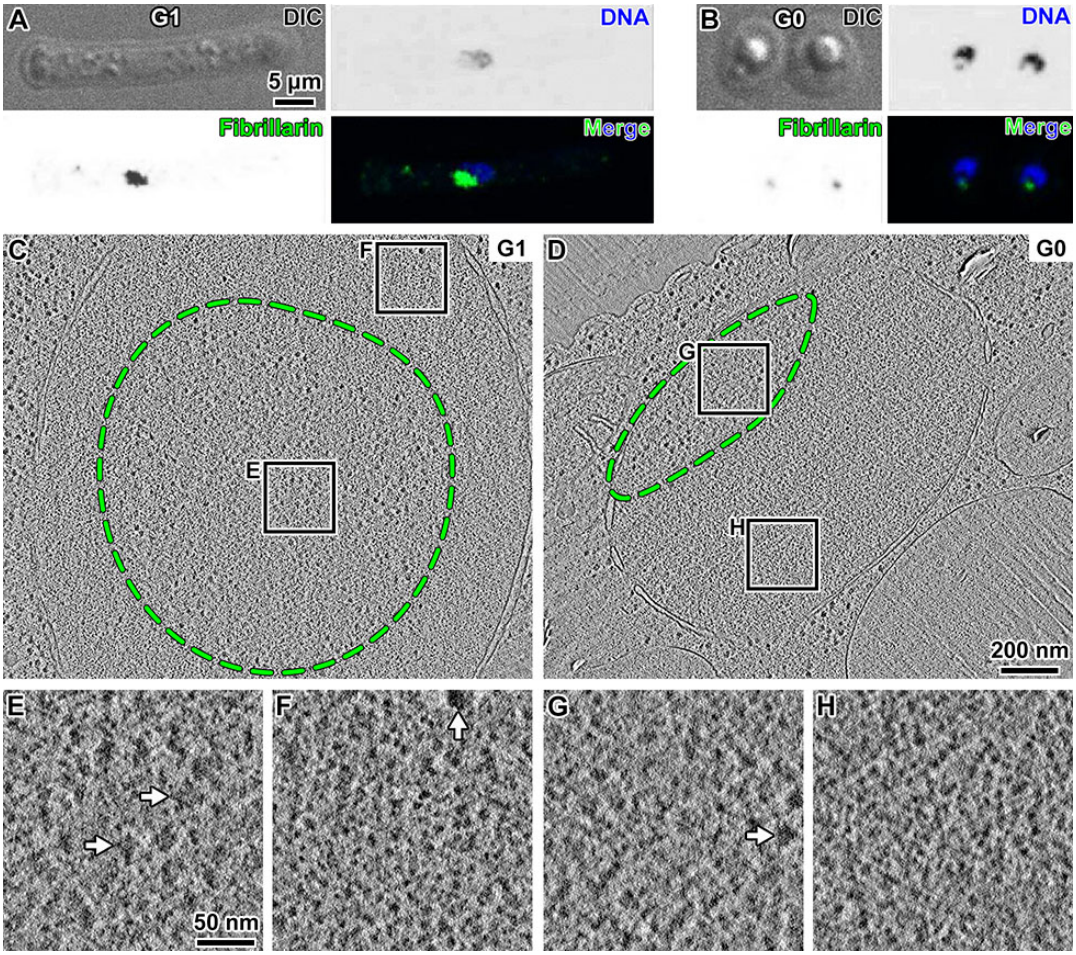

Figure 3. G0 megacomplexes are predominantly nucleolar. (A and B) Immunofluorescence detection of nucleoli in G1 and G0 cells. DAPI (blue) marks DNA and anti-fibrillarin antibody (green) marks the nucleolus. (C and D) Volta cryotomographic 25-nm slices of a G1 and a G0 cell, respectively. The area enclosed by the green dashed line denotes the approximate nucleolar boundary. Note that the nucleus in panel C was probably sectioned at a position where the nucleolus protrudes into the chromatin. In panel D, the high-contrast linear features running from 10 to 4 o'clock are knife marks. (E and F) Four-fold enlargements of the G1 nucleolar and chromatin positions boxed in panel C. (G and H) Four-fold enlargements of the G0 nucleolar and chromatin positions boxed in panel G. Example megacomplexes are indicated by arrows in panels E, F, and G.

hours of nitrogen starvation or in interphase and mitotic cells. The distribution of megacomplexes and nucleosome-like particles in G0-20d cells is indistinguishable from G0 cells. Because the contrast is so low in G0-20d cryotomograms, we did not pursue classification analysis on the nucleosome-like particles.

Histone deacetylation and G0 chromatin compaction are correlated

Previous studies showed that G0 *S. cerevisiae* cells have lower levels of several histone marks[30,31], including lower histone acetylation, which is correlated with oligonucleosome compaction[32-34]. We performed immunoblots and found that compared to G1 cells, *S. pombe* G0 cells have decreased levels of H3 acetylated at multiple N-terminal tail lysines (H3-Ac), but not H4 acetylated at multiple N-terminal tail lysines (H4-Ac) or at K16

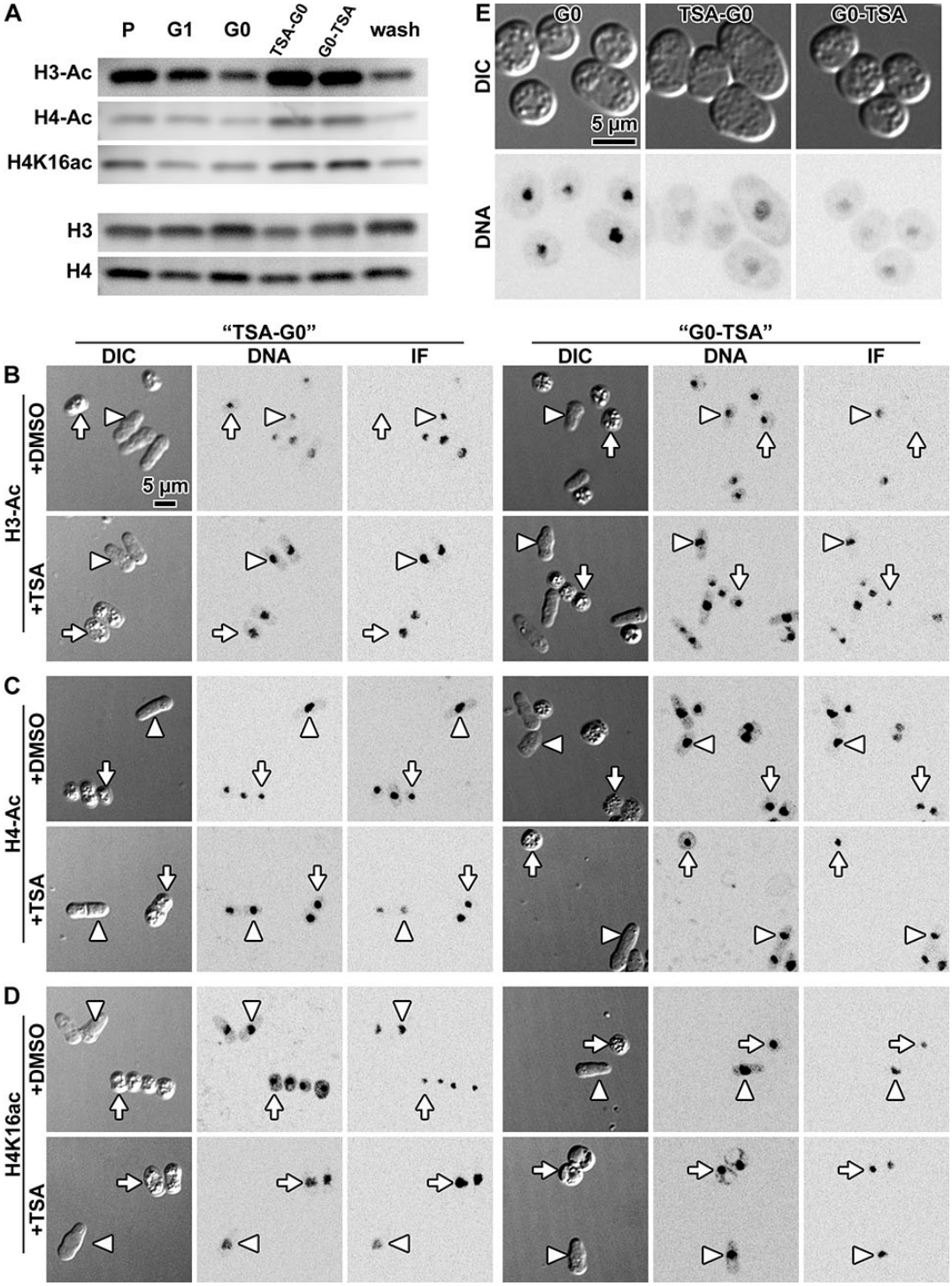

Figure 4. Histone H3 acetylation levels decrease in G0. (A) Immunoblots of *S. pombe* lysates from proliferating (P), G1, and G0 cells. The G0 cells were either untreated (G0), incubated with TSA in EMM−N for 24 hours (TSA-G0), incubated 24 hours in EMM−N followed by 24 hours of EMM−N plus TSA (G0-TSA), or treated with EMM−N plus TSA for 24 hours followed by TSA washout and then incubated an additional 24 hours in EMM−N (wash). Loading controls were done with antibodies against the H3 or H4 C-terminus. The uncropped immunoblots are shown in Figure S7. G0 cells were subjected to immunofluorescence imaging to detect (B) H3-Ac, (C) H4-Ac, and (D) H4K16ac. The G0 cells were treated with DMSO (+DMSO) or TSA (+TSA). "TSA-G0" and "G0-TSA" denote TSA treatment during or 24 hours after G0 entry, respectively, like in the immunoblot experiment. To minimize experimental variability, the G0 cells were fixed and then mixed with untreated fixed proliferating cells prior to immunofluorescence processing. The proliferating cells serve as a common reference. In each subpanel, one G0 cell is indicated by an arrow and one proliferating cell is indicated by an arrowhead. (E) DIC and fluorescence microscopy of untreated G0 cells and G0 cells that were treated with TSA during (TSA-G0) or 24 hours after G0 entry (G0-TSA). Note that some G0 cells are clumped together and appear as a bi-nucleated cell in the DAPI channel.

(H4K16ac) (Figure 4A). Combined with our immunofluorescence of CTD-S2P and 5-EU incorporation, our data are consistent with previous findings that at least one form of histone acetylation (H3) is correlated with transcriptionally active chromatin[35]. Because immunoblots show population-averaged histone-mark levels, we performed immunofluorescence to determine if there was cell-to-cell variability. We found that nearly all G0 cells have lower levels of histone H3 acetylation (Figure 4B). In contrast, neither H4 nor H4K16 acetylation decrease as much when compared to G1 cells (Figure 4, C and D). Nevertheless, both the immunoblots and immunofluorescence experiments show that overall histone acetylation decreases mildly in G0.

G0 chromatin compaction is decoupled from transcriptional repression

Trichostatin A (TSA) is a histone-deacetylase inhibitor that increases histone acetylation levels in proliferating *S. pombe* cells[36] and induces chromatin decompaction *in situ*[37,38]. To determine if TSA affects G0 chromatin and if these changes depend on the timing of TSA treatment, we subjected these cells to two TSA-treatment regimens. In the TSA-G0 regimen, we incubated proliferating cells in EMM−N plus TSA for 24 hours. In the G0-TSA regimen, we first incubated proliferating cells in EMM−N for 24 hours, then we incubated the cells in EMM−N plus TSA for another 24 hours. Immunoblots (Figure 4A) and immunofluorescence microscopy (Figure 4, B - D) showed that both TSA-G0 and G0-TSA cells have more H3 and H4 acetylation than untreated cells – even more than proliferating cells. TSA-induced G0 histone hyperacetylation is reversible because the acetylation levels dropped to untreated levels after we washed out the TSA from TSA-G0 cells. Curiously, cells are longer and their nuclei are larger when they are treated with TSA during G0 entry (TSA-G0), but not when treated with TSA after G0 entry (Figure 4E), meaning that chromatin is less compact in TSA-G0.

TSA-G0 cells allowed us to test if there is a correlation between a chromatin compaction-related histone mark, chromatin compaction *in situ*, transcription, and G0 thermotolerance. Cryotomograms revealed that TSA-G0 cells also have a dense nucleoplasm (Figure 5, A - D), making the classification and packing analysis of nucleosome-like particles unfeasible. Megacomplex concentrations in TSA-G0 chromatin was similar to G0 (Figure 5, B and D; Figure 2 E; average = 190 megacomplexes / femtoliter, $p = 0.2$). TSA-G0 cells are also thermotolerant (Figure S6A) and their CTD-S2P and 5-EU signals are barely detectable (Figure S6, B and C). These two G0 phenotypes are therefore

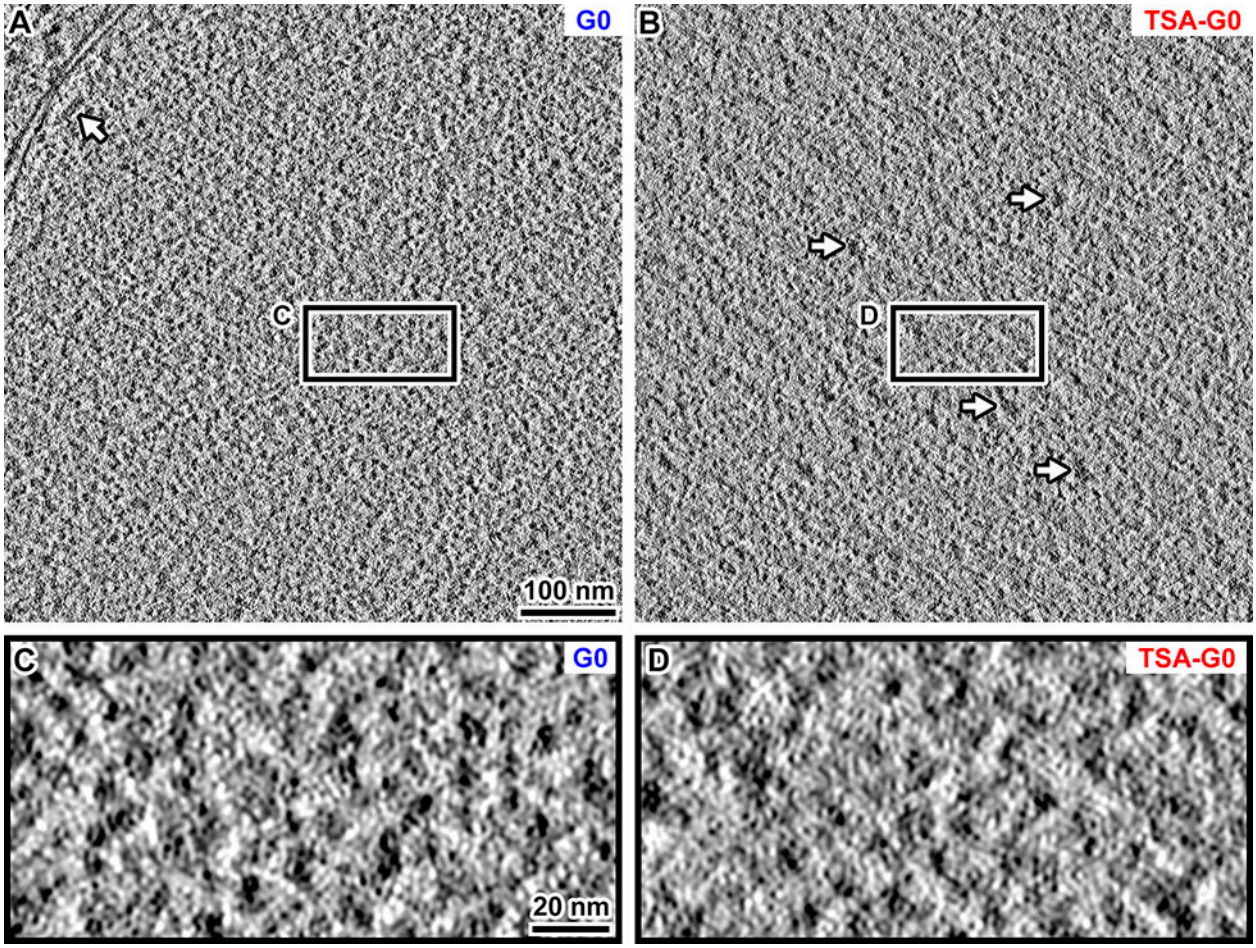

Figure 5. TSA-treated G0 cells also have a dense nucleoplasm. (A and B) Volta cryotomographic 10-nm slices of nuclei in a G0 cell and in a cell treated with TSA during G0 entry, respectively. The arrows indicate nuclear megacomplexes. Note that the cell in panel B contains more megacomplexes than the other TSA-G0 cells, which have megacomplex concentrations similar to that of G0 cells. (C and D) Four-fold enlargements of the positions boxed in panels A and B, respectively.

unaffected by histone hyperacetylation and non-compacted chromatin.

Discussion

It has been known for ~ 60 years that mitotic chromosome condensation is correlated with transcriptional repression[39,40]. Studies in the past two decades have since shown that this repression is not absolute because transcription factors can still access the interior of mitotic chromosomes[41-43] and because low-level transcription is detectable in mitotic mammalian cells[44-46]. In *S. pombe* G0 cells, we also observed a correlation between smaller nucleus size (a proxy for chromatin condensation) and transcriptional repression, in line with previous studies[8,10]. What we did not anticipate was a decrease in the concentration of megacomplexes associated with G0 chromatin. We previously observed that the abundance of megacomplexes in the chromatin is correlated with transcriptional activity in a comparison of G2 and prometaphase cells[11]. Therefore, in *S. pombe*, the abundance of megacomplexes may be a structural cell-biology marker for transcriptional activity.

We expected that G0 chromatin, which is the most transcriptionally repressed chromatin studied *in situ* by cryo-ET, would be much more compact than what we observed. In G0 cells, we did not observe chromatin packed into either ultra-compact structures or ordered fibers. This observation is consistent with all previous *in situ* cryo-EM and cryo-ET studies of eukaryotic cell nuclei[11,15,47-52]. Thus far, the most compact forms of natural chromatin studied by electron microscopy are the samples that are released from lysed nuclei[11,27,53], reconstituted arrays in the presence of divalent cations[54], and 30-nm fibers in isolated chicken erythrocyte nuclei[55]. The released yeast chromatin is so compact that individual nucleosomes cannot be resolved because they are aggregated in a large amorphous mass. Therefore, the biochemical environment inside yeast cell nuclei – even in G0 – limits the degree of chromatin compaction.

S. pombe natural G0 chromatin compaction is weakly correlated with histone deacetylation (Figure 6A). When they are treated with TSA, G0 histones become hyperacetylated. In TSA-G0 cells, the chromatin is not compacted, but the transcription remains repressed, meaning that chromatin compaction is not necessary for transcriptional repression in G0 *S. pombe*. This TSA-G0 phenotype adds to the growing body of counter-intuitive nuclear phenomena. For example, G0 B cells and mitotic yeast cells have more compact chromatin than proliferating and interphase cells, respectively, but they also have lower short-range Hi-C contact probabilities[56,57]. Time-resolved single-nucleosome tracking of RPE-1 cells has also shown that G0 phase chromatin is more dynamic than proliferating cell chromatin[58]. These counter-intuitive observations reflect our incomplete understanding of the many factors that influence chromatin structure and function *in situ*[59]. Such factors include Structural Maintenance of Chromosomes proteins, which contribute to budding yeast and T-cell G0 chromatin organization[60,61]; magnesium ions, which contribute to mammalian mitotic chromosome condensation[62]; and perhaps the nuclear envelope, which allows a 12-megabase genome to reside in a less-compact form in the larger nucleus of the fission yeast *S. japonicus*[63,64]

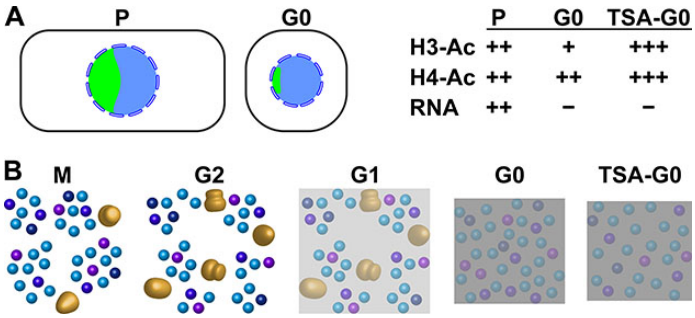

Figure 6: G0 nucleus phenotypes are not correlated with chromatin compaction or acetylation. (A) Cartoon of the cytological differences between proliferating (P) and G0 cells. Aside from having a smaller nucleus (blue circle), G0 cells have a disproportionately smaller nucleolus (green). Histone acetylation levels (H3-Ac and H4-Ac) are upregulated in G0 cells treated with histone-deacetylase inhibitor (TSA-G0). Transcription levels (RNA) are uncorrelated with changes in G0 histone acetylation. (B) Schematic of chromatin packing changes in mitotic (M), G2, G1, G0, and TSA-G0 cells. Megacomplexes (gold irregular objects) and nucleosome-like particles (spheres) are indicated. Megacomplexes are depicted with different shapes to reflect their conformational and constitutional diversity. The nucleosome-like particles are depicted with multiple colors because their exact identities are unknown. For G1, G0, and TSA-G0, the background is shown in gray and the complexes are shaded in washed-out colors to reflect the dense nucleoplasm and the uncertainty of the nuclear macromolecular packing.

In conclusion, *S. pombe* G0 and mitotic chromatin both have fewer nuclear megacomplexes than interphase cells (Figure 6B). Furthermore, G0 cells have such a dense nucleoplasm that their chromatin packing at the macromolecular level remains mysterious. Newer cryo-ET hardware, sample-preparation, and image-processing technologies may help reveal differences at the level of oligonucleosome clustering and folding[11,51]

Materials and Methods

Cell culture and synchronization

Proliferating wild-type 972 h- cells (strain MBY99) were grown in Edinburgh Minimal Medium (EMM, USBio, Salem, MA) or in yeast extract with supplements (YES) at 30°C (shaken at 200 - 250 RPM for all cell culture experiments) to OD_{600} = 0.2. Most cell washes were done by pelleting the cells by centrifugation, followed by resuspension in fresh growth media or buffer. To prepare G0 cells, proliferating cells were washed twice in EMM without nitrogen (EMM−N) and then incubated for 24 hours in EMM−N at 30°C. G0-20d cells were incubated in EMM−N for 20 days. For experiments with *cdc10-129* (strain MBY165; *leu1-32*) cells, the cultures were grown in EMM with added leucine or in YES at 30°C. When the OD_{600} reached 0.2, the cultures were transferred to 36°C and incubated for 4 hours, which arrests the majority of cells in G1 phase. For G0 experiments, wild-type or yFS240 cells were used because *cdc10-129* cells incubated in EMM−N with leucine did not become rounded. We believe this phenotype is a consequence of the strain's dependence on leucine supplements, which may act as a sufficient source of nitrogen that prevents G0 entry.

TSA perturbation

TSA (T8552, Sigma, Merck KGaA, Darmstadt, Germany) was prepared as a 1 mg/mL stock solution in DMSO. Cells growing in YES or EMM−N were pelleted and then TSA was added following two different regimens. For G0-TSA, proliferating cells were first incubated 24 hours in EMM−N, then 1 mg/mL TSA was added to 20 µg/mL final concentration (50 µg/mL for cryo-ET samples); cells had the same hyperacetylation phenotype after both 20 and 50 µg/mL TSA treatments. These cells were then incubated in TSA for 24 hours. For TSA-G0, proliferating cells were resuspended in EMM−N, then 1 mg/mL TSA was immediately added to 20 µg/mL final concentration. These cells were incubated for 24 hours. For the washout control, TSA-G0 cells were washed with fresh EMM−N, then incubated 24 hours before immunoblot processing.

Thermotolerance tests

Cells (OD_{600} range = 0.2 - 1.0 for proliferating, 0.7 for G0, 0.5 for TSA-G0, and 1.8 for G0-20d cells) (0.01 OD_{600} units per sample) were pelleted at 5,000 × g for 1 minute. The cell pellets were resuspended in 100 µL of 30°C or 48°C YES or EMM−N medium (from 1 mL prewarmed stock) and then immediately placed in either a 30°C shaking incubator or a 48°C heating block, respectively, then incubated for 30 minutes. The 48°C-heated cells were then cooled on ice for 1 minute. Four serial dilutions (10×, 100×, 1,000×, 10,000×) were made for each sample into YES to 45 µL total volume. The undiluted stock and diluted cultures (5 µl each) were spotted on a dry YES agar plate. Once the cells were adsorbed onto the agar (~ 30 minutes), the plates were turned upside down, sealed with Parafilm®, incubated at 30°C for 2 days, and then photographed.

DAPI staining (not for immunofluorescence)

For microscopy of DAPI-stained nuclei, cells were grown in EMM because DAPI signal is harder to see in YES-grown cells. Proliferating cells (0.5 OD_{600} units) were concentrated by pelleting at 5,000 × g for 1 minute and then resuspended in 1 mL EMM. G0 cell cultures started at OD_{600} = 0.2 and sometimes grew to OD_{600} > 0.5 after 24 hours of nitrogen starvation. These cultures were diluted to OD_{600} = 0.5 with EMM−N. Cell cultures were fixed by adding 37% formaldehyde (#47608-1L-F, Sigma) to 3.7% final concentration, incubated for 90 minutes (all fixation was done 200 - 250 RPM shaking), then collected by centrifugation at 5,000 × g for 1 minute. Cells were then washed twice in phosphate-buffered saline, pH 7.4 (PBS; Vivantis, Selangor Darul Ehsan, Malaysia) and resuspended in 20 µL of PBS with 1 µg/mL DAPI. Five µl of this sample was then added to a microscope slide and imaged using an Ultraview Vox spinning-disc confocal microscope (PerkinElmer, Waltham, MA) with a 60× objective lens.

Immunofluorescence microscopy

Indirect immunofluorescence microscopy was done using a modified version of our previous protocol[11] as follows. Proliferating, G1, and G0 cells were fixed with 3.7% formaldehyde for 90 minutes at 30°C. Cells were collected by centrifugation at 5,000 × g for 5 minutes and were then resuspended in 1 mL PEM (100 mM PIPES, 1 mM EGTA, 1 mM $MgSO_4$, pH 6.9) buffer. The cells were then washed once by centrifugation and resuspension with PEM, followed by resuspension in 1 mL PEMS (1.2 M sorbitol in PEM). Next, the cells were converted to spheroplasts with 25 U/mL Zymolyase (Zymo Research, Irvine, CA) in PEMS and incubated for 75 minutes in a 37°C water bath. All subsequent incubations were done at 10 RPM in a rotator (Invitrogen HulaMixer™). The cells were washed again with PEMS, resuspended in PEMS with 1% Triton X-100 (Sigma) and incubated at 22°C for 5 minutes. Cells were then washed twice with PEM and then incubated in PEMBAL (PEM, 1% BSA, 100 mM l-lysine hydrochloride) for 1 hour at 22°C. The primary and secondary antibodies used for immunostaining are listed in Table S1. The cells were resuspended in 100 µL of primary antibody diluted in PEMBAL to the dilution indicated in Table S1, and incubated at 22°C overnight. Next, the cells were washed twice with PEMBAL and resuspended in 100 µL of secondary antibody diluted in PEMBAL to the dilution indicated in Table S1 and then incubated at 22°C in the dark overnight. Finally, the cells were washed in PEM, then PBS, then resuspended in 20 µL of DAPI diluted to 1 µg/mL in PBS. Five µl of the sample was then added to a microscope slide and imaged using an Ultraview Vox spinning-disc confocal microscope. The images were recorded using either a 60× or a 100× objective lens.

Nascent RNA detection

Newly synthesized RNA was detected *in situ* using a 5-EU click-chemistry kit ("Click-iT™" C10329, Thermo Fisher Scientific, Waltham, MA). As a negative control, the RNA-polymerase inhibitor phenanthroline (20 mg/mL stock in deionized water, P9375, Sigma) was added to 1 mL cell culture to a final concentration of 350 µg/mL. Five-ethynyl uridine (100 mM stock in deionized water) was added to the cultures of strain yFS240 or to strain 972 h- (the control strain) to 1 mM final concentration and incubated at 30°C in the dark with shaking at 250 RPM for the various durations indicated in the results. Cells were then fixed with 1 mL of 3.7% formaldehyde in PBS for 15 minutes at 22°C; all subsequent incubations were done at 10 RPM in a rotator. Next, the cells were washed once by pelleting at 1,500 × g and resuspending in 1 mL of PBS. The cells were permeabilized with 1 mL of 0.5% Triton X-100 in PBS for 15 minutes at 22°C in the dark and then washed in PBS. Then the cells were treated with a reaction cocktail made with 428 µL of Click-iT RNA reaction buffer, 20 µL of 100 mM $CuSO_4$, 1.8 µL of Alexa Fluor® 488 stock solution and 50 µL of Click-iT reaction buffer additive as directed in the Click-iT RNA Alexa Fluor 488 Imaging Kit. This mixture was incubated at 22°C in the dark for 30 minutes. Finally, the labelled cells were washed in Click-iT reaction rinse buffer before they were resuspended in 20 µL of DAPI diluted to 1 µg/mL in PBS.

Immunoblots

Immunoblot samples were prepared using trichloroacetic acid (TCA) precipitation. The cell pellet (7 - 21 OD_{600} units, subsequently diluted to obtain equal protein loading) was resuspended in 200 µL of 20% TCA on ice. Approximately 0.4 g of glass beads (425 - 600 µm, Sigma) was added to the mixture. The cells were then vortexed for 1 minute, followed by incubation on ice for 1 minute; this vortex-incubation treatment was done four times in total. The cell lysate was then centrifuged at 2,000 × g for 10 seconds to sediment the glass beads. Next, 500 µL ice-cold 5% TCA was mixed with the lysate. The mixture (without glass beads) was transferred to a new tube. Another 500 µL of 5% ice-cold TCA was mixed with the glass beads and this new mixture (without glass beads) was added to the tube in the previous step. The combined mixture was then placed on ice for 10 minutes to precipitate proteins. Then the precipitated proteins were pelleted at 4°C, 15,000 × g for 20 minutes. The supernatant was removed and the pellet was re-centrifuged (either short-spin for 3 seconds or 15,000 × g for 1 minute), followed by the removal of the residual supernatant. The pellet was resuspended in 212 µL of 1× Laemmli sample buffer, followed by the immediate addition of 26 µL of 1 M Tris pH 8 to neutralize the residual TCA. Then the lysates were heated at 100°C for 5 minutes. The lysates were then centrifuged at 15,000 × g for 10 minutes and the clarified supernatant containing solubilized proteins was transferred to a new tube.

Protein loading levels were calibrated using immunoblots against both histone H3 and H4 C-termini. SDS-PAGE was done with Mini-PROTEAN® TGX™ 4-15% Precast Gels (Bio-Rad, Hercules, CA), electrophoresed for 90 minutes at 80 volts. Precision Plus Protein™ WesternC™ Standards (Bio-Rad) (2.5 µL) were loaded as molecular-weight markers. The proteins were then transferred to PVDF membrane (Bio-Rad Immun-Blot®) at 100 volts for 30 minutes at 4°C. The membrane was blocked in 2% BSA in TBS-T (TBS with 0.05% tween-20) for 1 hour at 22°C and then incubated with primary antibody overnight at 22°C. Next, the blot was rinsed 3 times in TBS-T and incubated with StrepTactin-HRP conjugate (Bio-Rad) and HRP-conjugated secondary antibody for 1 hour at 22°C. The blot was then rinsed 3 times in TBS-T. Chemiluminescence substrate was then applied to the blot according to the manufacturer's instructions (Bio-Rad Clarity™ Western ECL Substrate kit). The chemiluminescent signals were recorded using a Syngene G:BOX (Synoptics, Cambridge, United Kingdom). Uncropped immunoblots are shown in Figure S7.

Self-pressurized freezing

Self-pressurized freezing was adapted from a published method[65] as follows. Proliferating and G0 cells were pelleted by centrifuging at 1,000 × g for 5 minutes. A 60% w/v 40-kDa dextran (Sigma) stock solution in PBS was added to the cell pellet as an extracellular cryoprotectant to 30% final concentration. The cell/dextran mixture was quick spun to remove bubbles and then loaded into a copper tube (0.45 mm outer diameter and 0.3 mm inner diameter) with a syringe-type filler device (Part 733-1, Engineering Office M. Wohlwend GmbH, Sennwald, Switzerland). The tube was sealed by crimping both ends with flat-jaw pliers, held horizontally 3 cm above a pool of liquid ethane in a Vitrobot cup (Thermo Fisher Scientific), then dropped in. The flattened ends of the tube were removed with a tube cut device (Part. 732, Engineering Office M. Wohlwend GmbH), operated in liquid nitrogen.

Vitreous sectioning

Vitreous sectioning (cryosectioning) was performed with dual micromanipulators[66,67]. A continuous-carbon EM grid (CF200-Cu-50, EMS, Hatfield, PA) was coated with 5 µl colloidal-gold solution (5.7 x 10^{12} particles/mL 10-nm gold colloid; EM.GC10, BBI Solutions, Cardiff, United Kingdom) made in 0.1 mg/mL BSA (Sigma). These grids were then air dried at least one day prior to cryosectioning. Frozen-hydrated cells were cut into 70- or 100-nm thick cryo-ribbons using a 35° diamond knife (Cryo35, Diatome, Nidau, Switzerland) in a cryo-ultramicrotome (UC7/FC7, Leica Microsystems, Vienna, Austria) cooled to −150°C. Once the ribbon was ~ 3-mm long, the EM grid was positioned underneath the ribbon. To minimize the blockage at high tilt by grid bars, the grid was pre-oriented with its bars parallel to and flanking the ribbon. The ribbon was then attached to the grid by operating the Crion (Leica) in "charge" mode for 30 seconds. The grid was then stored in liquid nitrogen until imaging.

Electron cryotomography

Tilt series were collected using FEI TOMO4 on a Titan Krios cryo-TEM (Thermo Fisher Scientific) operated at 300 kV. This microscope is equipped with a Volta phase-plate, and a Falcon II direct-detection camera. Details of the imaging parameters are shown in Table S2. The tilt series were automatically coarse aligned using the IMOD program *Etomo* running in batch-tomography mode[68-70]. Image fine alignment was done using the colloidal gold particles as fiducial markers. Contrast-transfer function compensation was done for the few defocus phase-contrast images, but not for the Volta phase-contrast images. To suppress the high-spatial-frequency noise, the tilt series were low-pass filtered with a gentle Gaussian roll off starting at ~ 30 Å resolution (Etomo 2-D filter parameters $\mu = 0.15$, and $\sigma = 0.05$ for 4.6 Å pixel size). Cryotomograms were reconstructed by weighted back projection using the default Etomo parameters, then trimmed in 3-D to exclude features outside the field of interest.

Template matching

Template matching was done using the PEET package (Particle Estimation for Electron Tomography)[71,72]. Either a subtomogram of a nucleosome-like particle or a rounded 10-nm-wide, 6-nm-thick cylinder was used as a template. This template was enclosed with a spherical mask of either 6.2 or 7.5 nm radius. The different choices of templates and masks did not affect the filtered set because a low cross-correlation cutoff of 0.2 was used, which results in many false positives that are removed during 2-D classification[11]. A rectangular search grid with a 10-nm spacing was generated with the PEET program *gridInit*. Because this grid extended into the cytoplasm, a nucleus-enclosing boundary model was created within the same grid model file. This boundary model was drawn along the nuclear envelope at the "top" and "bottom" of the cryotomogram. The search points outside the nucleus were excluded with the IMOD command "clipmodel -bound 2 original.mod new.mod". Template-matching hits that were within 6 nm of each other were considered as duplicates. One of the duplicates was automatically removed.

Classification analysis of nucleosome-like particles

All scripts prefixed by ot_ are available at https://github.com/anaphaze/ot-tools. Classification in 2-D was done with either RELION 2.1 or RELION 3.0 (REgularised LIkelihood OptimisatioN)[73,74], using the subtomogram-analysis routines[26]. The G0 and G1 nucleosome-like particles' centers of mass were converted from a PEET .mod file to a text file with the IMOD program *model2point*. These positions were then read into RELION to extract subtomograms with a 16.6 nm box size. A 12-nm-thick cryotomographic slice was generated from each subtomogram using the script *ot_relion_project.py*. These slices were then subjected to sequential rounds of 2-D classification, using a 140 Å circular mask in the first round and a 120 Å circular mask in subsequent rounds, all with a 35 Å-resolution cutoff. All other parameters were kept to the RELION defaults. Changes to the resolution and the T parameters did not make the classification choices less ambiguous.

Megacomplex analysis

To facilitate megacomplex picking, Volta cryotomograms were binned twofold in 3-D with the IMOD program *binvol*. Each cryotomogram was opened with the 3dmod *slicer* tool set to ~ 30-nm-thick tomographic slices. Nuclear particles that were (1) larger than 15 nm and (2) outside the nucleolus were picked as "scattered" contour points. To estimate the chromatin volume, a "closed" contour was drawn around the chromatin position at the central slice of the cryotomogram. The area within this contour was calculated using the IMOD command "imodinfo -F model.mod". This method reports the contour's "Cylinder Volume", defined in this case as Area × pixel_size^3, with Area expressed in voxels and pixel_size expressed in nanometers. This area was then multiplied by the tomogram thickness (in voxels) to estimate the volume.

Data sharing

Representative cryotomograms of one G0 cell and one G1 cell have been deposited as EMDB entry EMD-0875. All the tilt series and cryotomograms presented in this paper was deposited as EMPIAR[75] entry EMPIAR-10339. We focused our efforts on the highest-contrast cryo-ET data that contained nuclear positions, leaving a large number of tilt series unanalyzed. These surplus tilt-series and many corresponding cryotomograms were deposited with our yeast surplus-data[76] entry EMPIAR-10227.

Figure preparation and statistics

Image format interconversion and contrast adjustments were applied to the entire field of view using FIJI[77] or Adobe Photoshop (Adobe Systems, San Jose, CA). Student's t-tests were done with Google sheets (Alphabet Inc., Mountain View, CA). All cryotomogram analysis was done using the highest-contrast cryotomograms, which were selected from the best one or two cryosection ribbons, meaning that the analyzed data were technical replicates.

Author Contributions and Notes

SC, ZYT, LG - project design, experiments, analysis, writing; XN - project design, experiments; JS - training.

The authors declare no conflict of interest. This article contains supplementary information online.

Acknowledgments

We thank the CBIS microscopy staff for support and training. We thank Mohan Balasubramanian for strains MBY99 (972 h-) and MBY165 (*cdc10-129*); and Makoto Ohira and Nick Rhind for sharing and advising on the use of the TK-hENT strain yFS240. We thank the Finkelstein Lab for sharing their bioRχiv template. This work was supported by a Singapore Ministry of Education T2 MOE2018-T2-2-146 and a T1 R-154-000-B42-114 grant.

References

1 Kornberg, R. D. Chromatin structure: a repeating unit of histones and DNA. *Science* **184**, 868-871, doi:10.1126/science.184.4139.868 (1974).

2 Luger, K., Mäder, A. W., Richmond, R. K., Sargent, D. F. & Richmond, T. J. Crystal structure of the nucleosome core particle at 2.8 Å resolution. *Nature* **389**, 251-260 (1997).

3 Luger, K., Dechassa, M. L. & Tremethick, D. J. New insights into nucleosome and chromatin structure: an ordered state or a disordered affair? *Nat Rev Mol Cell Biol* **13**, 436-447, doi:10.1038/nrm3382 (2012).

4 Maeshima, K., Ide, S. & Babokhov, M. Dynamic chromatin organization without the 30-nm fiber. *Curr Opin Cell Biol* **58**, 95-104, doi:10.1016/j.ceb.2019.02.003 (2019).

5 Oomen, M. E. & Dekker, J. Epigenetic characteristics of the mitotic chromosome in 1D and 3D. *Crit Rev Biochem Mol Biol* **52**, 185-204, doi:10.1080/10409238.2017.1287160 (2017).

6 Nurse, P., Thuriaux, P. & Nasmyth, K. Genetic control of the cell division cycle in the fission yeast Schizosaccharomyces pombe. *Mol Gen Genet* **146**, 167-178 (1976).

7 Hiraoka, Y., Toda, T. & Yanagida, M. The NDA3 gene of fission yeast encodes beta-tubulin: a cold-sensitive nda3 mutation reversibly blocks spindle formation and chromosome movement in mitosis. *Cell* **39**, 349-358 (1984).

8 Su, S. S., Tanaka, Y., Samejima, I., Tanaka, K. & Yanagida, M. A nitrogen starvation-induced dormant G0 state in fission yeast: the establishment from uncommitted G1 state and its delay for return to proliferation. *J Cell Sci* **109 (Pt 6)**, 1347-1357 (1996).

9 Costello, G., Rodgers, L. & Beach, D. Fission yeast enters the stationary phase G0 state from either mitotic G1 or G2. *Current Genetics* **11**, 119-125 (1986).

10 Marguerat, S. *et al.* Quantitative analysis of fission yeast transcriptomes and proteomes in proliferating and quiescent cells. *Cell* **151**, 671-683, doi:10.1016/j.cell.2012.09.019 (2012).

11 Cai, S. *et al.* Cryo-ET reveals the macromolecular reorganization of S. pombe mitotic chromosomes in vivo. *Proc Natl Acad Sci U S A* **115**, 10977-10982, doi:10.1073/pnas.1720476115 (2018).

12 Aves, S. J., Durkacz, B. W., Carr, A. & Nurse, P. Cloning, sequencing and transcriptional control of the Schizosaccharomyces pombe cdc10 'start' gene. *EMBO J* **4**, 457-463 (1985).

13 Mochida, S. & Yanagida, M. Distinct modes of DNA damage response in S. pombe G0 and vegetative cells. *Genes Cells* **11**, 13-27, doi:10.1111/j.1365-2443.2005.00917.x (2006).

14 Forsburg, S. L. The best yeast? *Trends Genet* **15**, 340-344 (1999).

15 Gan, L., Ladinsky, M. S. & Jensen, G. J. Chromatin in a marine picoeukaryote is a disordered assemblage of nucleosomes. *Chromosoma* **122**, 377-386, doi:10.1007/s00412-013-0423-z (2013).

16 Sajiki, K. *et al.* Genetic control of cellular quiescence in S. pombe. *J Cell Sci* **122**, 1418-1429, doi:10.1242/jcs.046466 (2009).

17 Fukuda, Y., Laugks, U., Lucic, V., Baumeister, W. & Danev, R. Electron cryotomography of vitrified cells with a Volta phase plate. *J Struct Biol* **190**, 143-154, doi:10.1016/j.jsb.2015.03.004 (2015).

18 Asano, S. *et al.* Proteasomes. A molecular census of 26S proteasomes in intact neurons. *Science* **347**, 439-442, doi:10.1126/science.1261197 (2015).

19 Komarnitsky, P., Cho, E. J. & Buratowski, S. Different phosphorylated forms of RNA polymerase II and associated mRNA processing factors during transcription. *Genes Dev* **14**, 2452-2460 (2000).

20 Harlen, K. M. & Churchman, L. S. The code and beyond: transcription regulation by the RNA polymerase II carboxy-terminal domain. *Nat Rev Mol Cell Biol* **18**, 263-273, doi:10.1038/nrm.2017.10 (2017).

21 Sivakumar, S., Porter-Goff, M., Patel, P. K., Benoit, K. & Rhind, N. In vivo labeling of fission yeast DNA with thymidine and thymidine analogs. *Methods* **33**, 213-219, doi:10.1016/j.ymeth.2003.11.016 (2004).

22 Hodson, J. A., Bailis, J. M. & Forsburg, S. L. Efficient labeling of fission yeast Schizosaccharomyces pombe with thymidine and BUdR. *Nucleic Acids Res* **31**, e134 (2003).

23 Jao, C. Y. & Salic, A. Exploring RNA transcription and turnover in vivo by using click chemistry. *Proc Natl Acad Sci U S A* **105**, 15779-15784, doi:10.1073/pnas.0808480105 (2008).

24 Tanaka, K. & Kanbe, T. Mitosis in the fission yeast Schizosaccharomyces pombe as revealed by freeze-substitution electron microscopy. *J Cell Sci* **80**, 253-268 (1986).

25 Warner, J. R. The economics of ribosome biosynthesis in yeast. *Trends Biochem Sci* **24**, 437-440 (1999).

26 Bharat, T. A., Russo, C. J., Lowe, J., Passmore, L. A. & Scheres, S. H. Advances in Single-Particle Electron Cryomicroscopy Structure Determination applied to Sub-tomogram Averaging. *Structure* **23**, 1743-1753, doi:10.1016/j.str.2015.06.026 (2015).

27 Cai, S., Song, Y., Chen, C., Shi, J. & Gan, L. Natural chromatin is heterogeneous and self-associates in vitro. *Mol Biol Cell* **29**, 1652-1663, doi:10.1091/mbc.E17-07-0449 (2018).

28 Roche, B., Arcangioli, B. & Martienssen, R. A. RNA interference is essential for cellular quiescence. *Science* **354**, doi:10.1126/science.aah5651 (2016).

29 Li, L. *et al.* Key events during the transition from rapid growth to quiescence in budding yeast require posttranscriptional regulators. *Mol Biol Cell* **24**, 3697-3709, doi:10.1091/mbc.E13-05-0241 (2013).

30 Mews, P. *et al.* Histone methylation has dynamics distinct from those of histone acetylation in cell cycle reentry from quiescence. *Mol Cell Biol* **34**, 3968-3980, doi:10.1128/MCB.00763-14 (2014).

31 McKnight, J. N., Boerma, J. W., Breeden, L. L. & Tsukiyama, T. Global Promoter Targeting of a Conserved Lysine Deacetylase for Transcriptional Shutoff during Quiescence Entry. *Mol Cell* **59**, 732-743, doi:10.1016/j.molcel.2015.07.014 (2015).

32 Tse, C., Sera, T., Wolffe, A. P. & Hansen, J. C. Disruption of higher-order folding by core histone acetylation dramatically enhances transcription of nucleosomal arrays by RNA polymerase III. *Mol Cell Biol* **18**, 4629-4638 (1998).

33 Shogren-Knaak, M. *et al.* Histone H4-K16 acetylation controls chromatin structure and protein interactions. *Science* **311**, 844-847, doi:10.1126/science.1124000 (2006).

34 Robinson, P. J. *et al.* 30 nm chromatin fibre decompaction requires both H4-K16 acetylation and linker histone eviction. *J Mol Biol* **381**, 816-825, doi:10.1016/j.jmb.2008.04.050 (2008).

35 Dion, M. F., Altschuler, S. J., Wu, L. F. & Rando, O. J. Genomic characterization reveals a simple histone H4 acetylation code. *Proc Natl Acad Sci U S A* **102**, 5501-5506, doi:10.1073/pnas.0500136102 (2005).

36 Kimata, Y. *et al.* Diminishing HDACs by drugs or mutations promotes normal or abnormal sister chromatid separation by affecting APC/C and adherin. *J Cell Sci* **121**, 1107-1118, doi:10.1242/jcs.024224 (2008).

37 Rundlett, S. E. *et al.* HDA1 and RPD3 are members of distinct yeast histone deacetylase complexes that regulate silencing and transcription. *Proc Natl Acad Sci U S A* **93**, 14503-14508 (1996).

38 Toth, K. F. *et al.* Trichostatin A-induced histone acetylation causes decondensation of interphase chromatin. *J Cell Sci* **117**, 4277-4287, doi:10.1242/jcs.01293 (2004).

39 Taylor, J. H. Nucleic acid synthesis in relation to the cell division cycle. *Ann N Y Acad Sci* **90**, 409-421 (1960).

40 Prescott, D. M. & Bender, M. A. Synthesis of RNA and protein during mitosis in mammalian tissue culture cells. *Exp Cell Res* **26**, 260-268 (1962).

41 Chen, D. *et al.* Condensed mitotic chromatin is accessible to transcription factors and chromatin structural proteins. *J Cell Biol* **168**, 41-54, doi:10.1083/jcb.200407182 (2005).

42 Hsiung, C. C. *et al.* Genome accessibility is widely preserved and locally modulated during mitosis. *Genome Res* **25**, 213-225, doi:10.1101/gr.180646.114 (2015).

43 Teves, S. S. *et al.* A dynamic mode of mitotic bookmarking by transcription factors. *Elife* **5**, doi:10.7554/eLife.22280 (2016).

44 Liang, K. *et al.* Mitotic Transcriptional Activation: Clearance of Actively Engaged Pol II via Transcriptional Elongation Control in Mitosis. *Mol Cell* **60**, 435-445, doi:10.1016/j.molcel.2015.09.021 (2015).

45 Palozola, K. C. *et al.* Mitotic transcription and waves of gene reactivation during mitotic exit. *Science* **358**, 119-122, doi:10.1126/science.aal4671 (2017).

46 Teves, S. S. *et al.* A stable mode of bookmarking by TBP recruits RNA polymerase II to mitotic chromosomes. *Elife* **7**, doi:10.7554/eLife.35621 (2018).

47 McDowall, A. W., Smith, J. M. & Dubochet, J. Cryo-electron microscopy of vitrified chromosomes in situ. *EMBO J* **5**, 1395-1402 (1986).

48 Eltsov, M., MacLellan, K. M., Maeshima, K., Frangakis, A. S. & Dubochet, J. Analysis of cryo-electron microscopy images does not support the existence of 30-nm chromatin fibers in mitotic chromosomes in situ. *Proceedings of the National Academy of Sciences* **105**, 19732-19737 (2008).

49 Eltsov, M., Sosnovski, S., Olins, A. L. & Olins, D. E. ELCS in ice: cryo-electron microscopy of nuclear envelope-limited chromatin sheets. *Chromosoma* **123**, 303-312, doi:10.1007/s00412-014-0454-0 (2014).

50 Chen, C. *et al.* Budding yeast chromatin is dispersed in a crowded nucleoplasm in vivo. *Mol Biol Cell* **27**, 3357-3368, doi:10.1091/mbc.E16-07-0506 (2016).

51 Cai, S., Böck, D., Pilhofer, M. & Gan, L. The in situ structures of mono-, di-, and trinucleosomes in human heterochromatin. *Mol Biol Cell* **29**, 2450-2457, doi:10.1091/mbc.E18-05-0331 (2018).

52 Eltsov, M. *et al.* Nucleosome conformational variability in solution and in interphase nuclei evidenced by cryo-electron microscopy of vitreous sections. *Nucleic Acids Res* **46**, 9189-9200, doi:10.1093/nar/gky670 (2018).

53 Scheffer, M. P., Eltsov, M., Bednar, J. & Frangakis, A. S. Nucleosomes stacked with aligned dyad axes are found in native compact chromatin in vitro. *J Struct Biol* **178**, 207-214, doi:10.1016/j.jsb.2011.11.020 (2012).

54 Maeshima, K. *et al.* Nucleosomal arrays self-assemble into supramolecular globular structures lacking 30-nm fibers. *EMBO J* **35**, 1115-1132, doi:10.15252/embj.201592660 (2016).

55 Scheffer, M. P., Eltsov, M. & Frangakis, A. S. Evidence for short-range helical order in the 30-nm chromatin fibers of erythrocyte nuclei. *Proceedings of the National Academy of Sciences* **108**, 16992-16997 (2011).

56 Kieffer-Kwon, K. R. *et al.* Myc Regulates Chromatin Decompaction and Nuclear Architecture during B Cell Activation. *Mol Cell* **67**, 566-578 e510, doi:10.1016/j.molcel.2017.07.013 (2017).

57 Kakui, Y., Rabinowitz, A., Barry, D. J. & Uhlmann, F. Condensin-mediated remodeling of the mitotic chromatin landscape in fission yeast. *Nat Genet* **49**, 1553-1557, doi:10.1038/ng.3938 (2017).

58 Nagashima, R. *et al.* Single nucleosome imaging reveals loose genome chromatin networks via active RNA polymerase II. *J Cell Biol* **218**, 1511-1530, doi:10.1083/jcb.201811090 (2019).

59 Kruhlak, M. J. *et al.* Regulation of global acetylation in mitosis through loss of histone acetyltransferases and deacetylases from chromatin. *J Biol Chem* **276**, 38307-38319, doi:10.1074/jbc.M100290200 (2001).

60 Swygert, S. G. *et al.* Condensin-Dependent Chromatin Compaction Represses Transcription Globally during Quiescence. *Mol Cell* **73**, 533-546 e534, doi:10.1016/j.molcel.2018.11.020 (2019).

61 Rawlings, J. S., Gatzka, M., Thomas, P. G. & Ihle, J. N. Chromatin condensation via the condensin II complex is required for peripheral T-cell quiescence. *EMBO J* **30**, 263-276, doi:10.1038/emboj.2010.314 (2011).

62 Maeshima, K. *et al.* A Transient Rise in Free Mg(2+) Ions Released from ATP-Mg Hydrolysis Contributes to Mitotic Chromosome Condensation. *Current biology : CB* **28**, 444-451 e446, doi:10.1016/j.cub.2017.12.035 (2018).

63 Yam, C., He, Y., Zhang, D., Chiam, K. H. & Oliferenko, S. Divergent strategies for controlling the nuclear membrane satisfy geometric constraints during nuclear division. *Current biology : CB* **21**, 1314-1319, doi:10.1016/j.cub.2011.06.052 (2011).

64 Rhind, N. *et al.* Comparative functional genomics of the fission yeasts. *Science* **332**, 930-936, doi:10.1126/science.1203357 (2011).

65 Yakovlev, S. & Downing, K. H. Freezing in sealed capillaries for preparation of frozen hydratedsections. *J Microsc* **244**, 235-247, doi:10.1111/j.1365-2818.2011.03530.x (2011).

66 Ladinsky, M. S., Pierson, J. M. & McIntosh, J. R. Vitreous cryo-sectioning of cells facilitated by a micromanipulator. *J Microsc* **224**, 129-134, doi:10.1111/j.1365-2818.2006.01674.x (2006).

67 Studer, D., Klein, A., Iacovache, I., Gnaegi, H. & Zuber, B. A new tool based on two micromanipulators facilitates the handling of ultrathin cryosection ribbons. *J Struct Biol* **185**, 125-128, doi:10.1016/j.jsb.2013.11.005 (2014).

68 Kremer, J. R., Mastronarde, D. N. & McIntosh, J. R. Computer visualization of three-dimensional image data using IMOD. *Journal of Structural Biology* **116**, 71-76 (1996).

69 Mastronarde, D. N. Dual-axis tomography: an approach with alignment methods that preserve resolution. *J Struct Biol* **120**, 343-352, doi:10.1006/jsbi.1997.3919 (1997).

70 Mastronarde, D. N. & Held, S. R. Automated tilt series alignment and tomographic reconstruction in IMOD. *J Struct Biol* **197**, 102-113, doi:10.1016/j.jsb.2016.07.011 (2017).

71 Nicastro, D. *et al.* The molecular architecture of axonemes revealed by cryoelectron tomography. *Science* **313**, 944-948, doi:10.1126/science.1128618 (2006).

72 Heumann, J. M. *PEET*, <http://bio3d.colorado.edu/PEET/> (2016).

73 Kimanius, D., Forsberg, B. O., Scheres, S. H. & Lindahl, E. Accelerated cryo-EM structure determination with parallelisation using GPUs in RELION-2. *Elife* **5**, doi:10.7554/eLife.18722 (2016).

74 Zivanov, J. *et al.* New tools for automated high-resolution cryo-EM structure determination in RELION-3. *Elife* **7**, doi:10.7554/eLife.42166 (2018).

75 Iudin, A., Korir, P. K., Salavert-Torres, J., Kleywegt, G. J. & Patwardhan, A. EMPIAR: a public archive for raw electron microscopy image data. *Nature methods* **13**, 387-388, doi:10.1038/nmeth.3806 (2016).

76 Gan, L., Ng, C. T., Chen, C. & Cai, S. A collection of yeast cellular electron cryotomography data. *Gigascience* **8**, doi:10.1093/gigascience/giz077 (2019).

77 Schneider, C. A., Rasband, W. S. & Eliceiri, K. W. NIH Image to ImageJ: 25 years of image analysis. *Nature methods* **9**, 671-675 (2012).

Supplementary information

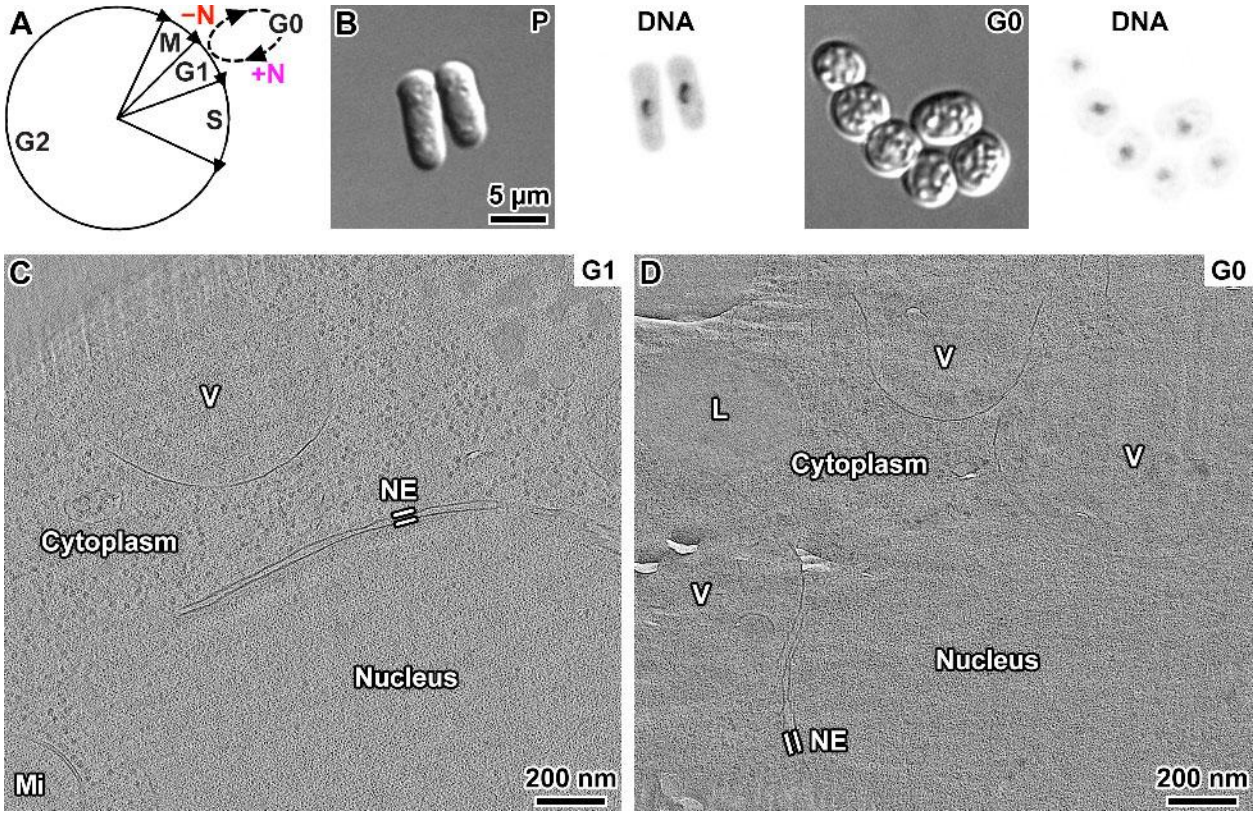

Figure S1: G0 cells undergo large-scale cytological remodeling. (A) Schematic of the *S. pombe* cell cycle: G1 phase, S phase, G2 phase, and Mitosis (M). Entry to and exit from G0 is shown with the dashed line and depends on the availability of nitrogen (+/− N). (B) DIC (left) and fluorescence (right, DNA) images of DAPI-stained proliferating (P) cells (most in G2 phase) and G0 cells. (C and D) Cryotomographic 30-nm slices of a G1-arrested and a G0 cell. NE: nuclear envelope. Mi: mitochondria. V: vacuole. L: lipid body. The parallel features resembling those in the upper-left corner of panel C and running from 12 to 6 o'clock are knife marks. The crescent-shaped features in panel D are cell structures that were damaged by cryomicrotomy.

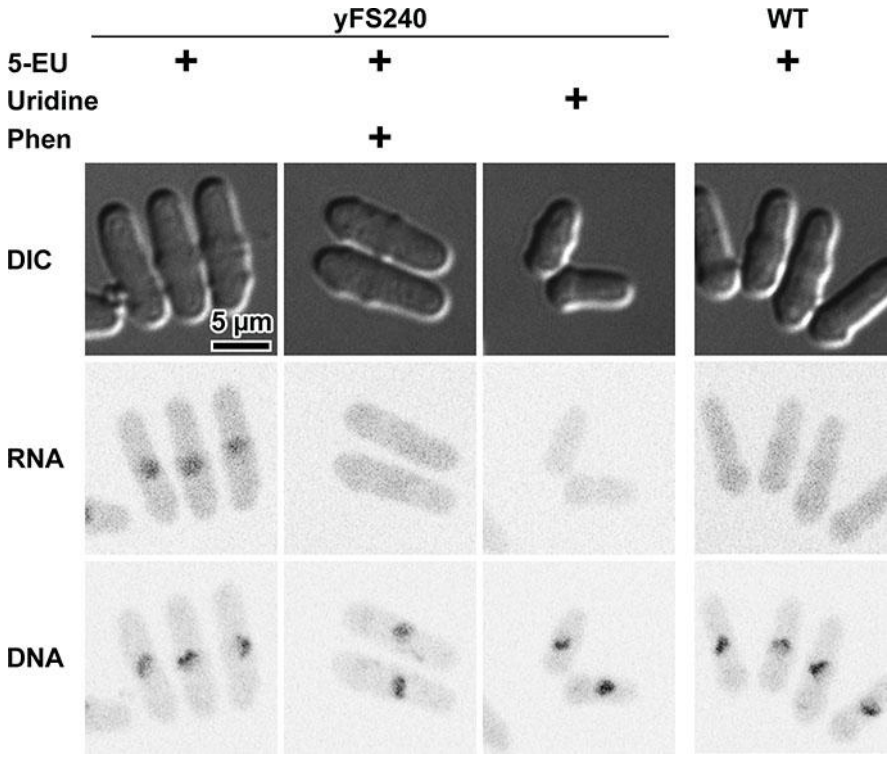

Figure S2. Controls for 5-EU RNA labeling. Proliferating yFS240 or wild-type cells incubated 10 minutes with 5-EU, uridine, or 5-EU plus the transcription inhibitor phenanthroline (Phen). The cells were then labeled with Alexa Fluor 488 and counterstained with DAPI.

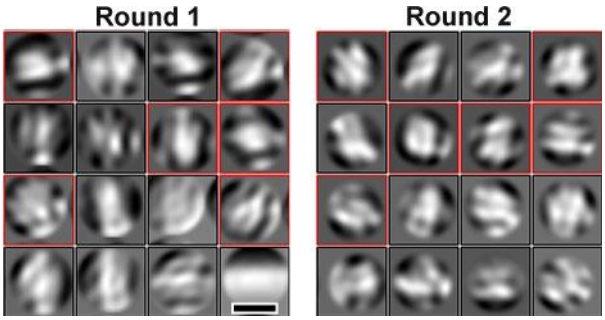

Figure S3. Low cryo-ET contrast makes G1 and G0 2-D class averages ambiguous. Nucleosome-like particle template-matching hits from G0 and G1 cells were converted to cryotomographic slices and subjected to 2-D classification. Example class averages from the first and second rounds of classification are shown. The nucleosome-like particles are boxed in red. A class average is deemed nucleosome-like if it has the approximate dimensions of a nucleosome that is viewed approximately along its “edge” (~ 6 nm x 10 nm) or “face” (~ 10 nm x 10 nm). Excluded class averages contain densities that span the mask, or are too small to be a nucleosome. Scale bar, 10 nm.

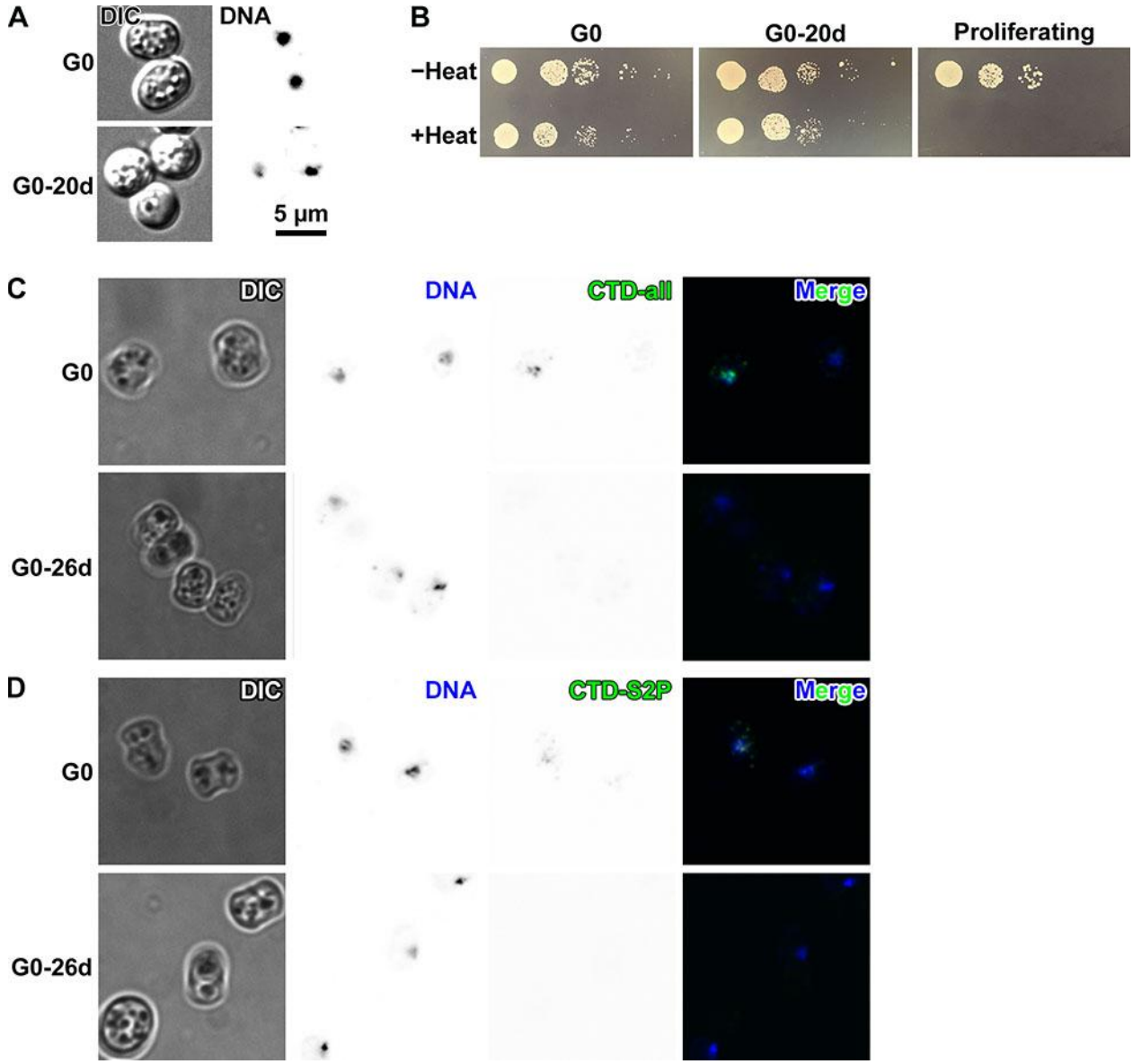

Figure S4. Transcription is further repressed in G0 "deep-quiescent" cells. (A) Light micrographs of DAPI-stained G0 and G0-20d cells. The lower G0-20d cell may be dead because it lacks both cytoplasmic DIC contrast and DAPI fluorescence. (B) Thermotolerance spot tests of G0, G0-20d, and proliferating cells (control). (C and D) Immunofluorescence of RNA Polymerase II CTD and CTD-S2P, respectively, in G0 and G0-26d cells; note that in this experiment, the deep-quiescent cells were kept in EMM−N 6 days longer.

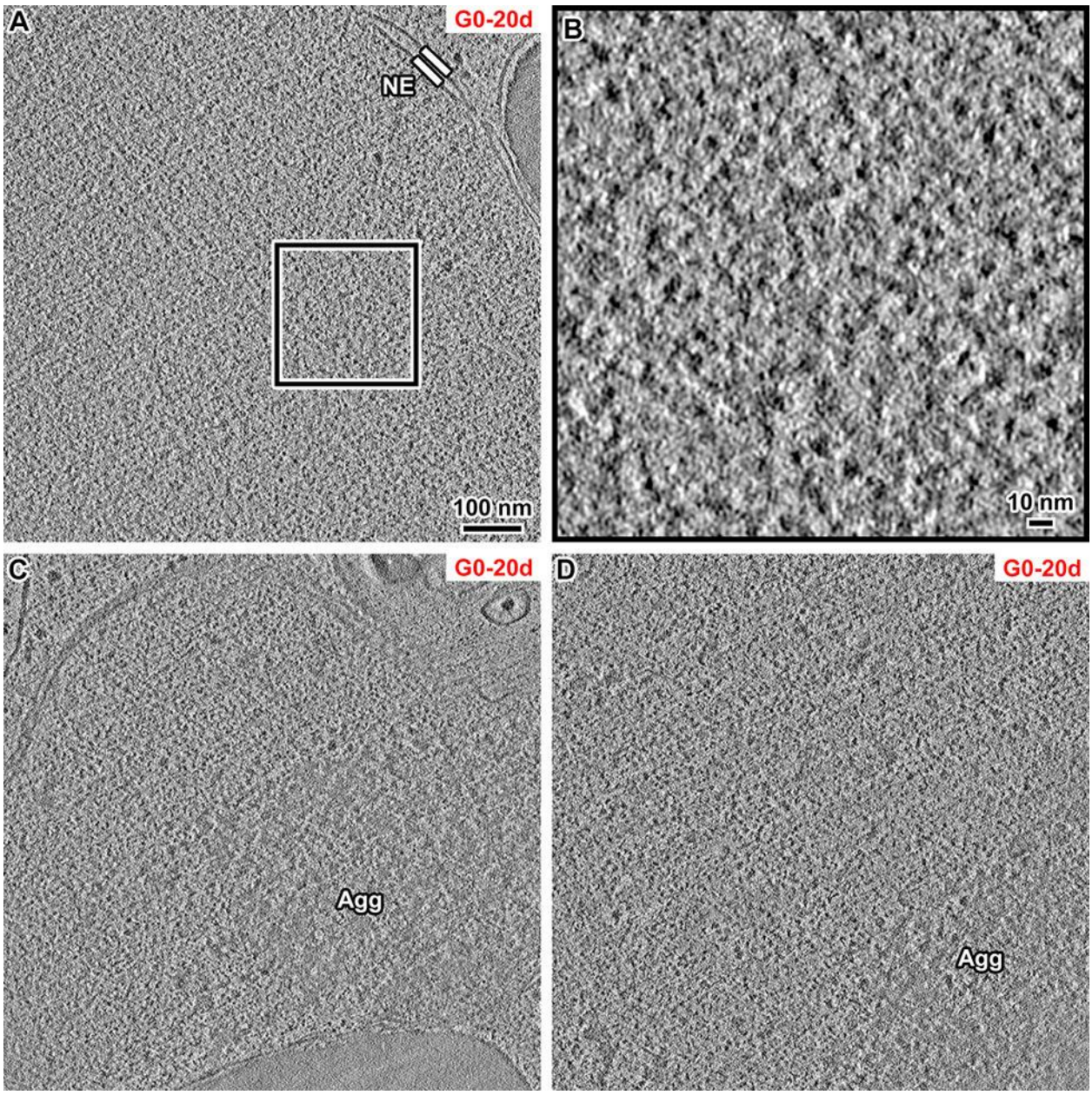

Figure S5. G0 "deep-quiescent" nuclei also have a dense nucleoplasm. (A) Volta cryotomographic 10-nm slices of a G0 cell, starved of nitrogen for 20 days (G0-20d). (B) Four-fold enlargement of the nuclear position boxed in panel A. (C and D) Examples of cells that have intranuclear aggregates, which are denoted by "Agg". The scale is the same as in panel A.

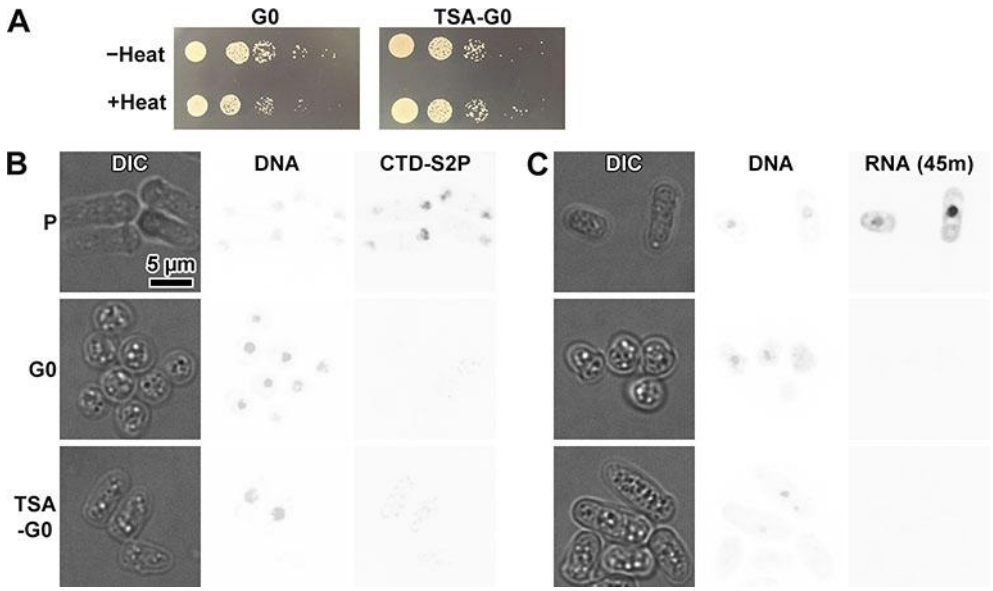

Figure S6. TSA treatment during G0 entry does not affect thermotolerance or transcriptional repression. (A) Spot tests of G0 and TSA-G0 cells after a 30-minute incubation in EMM−N, with and without heat stress. (B) DIC and fluorescence microscopy of proliferating (P), G0, and TSA-G0 wild-type cells. The cells were stained for DNA with DAPI and immunostained for RNA polymerase II with CTD-S2P. (C) DIC and fluorescence microscopy of proliferating (P), G0, and TSA-G0 yFS240 cells. The cells were incubated with 5-EU for 45 minutes to increase the amount of 5-EU incorporated into RNA. Nascent RNA was then ligated to Alexa Fluor 488 for fluorescence detection.

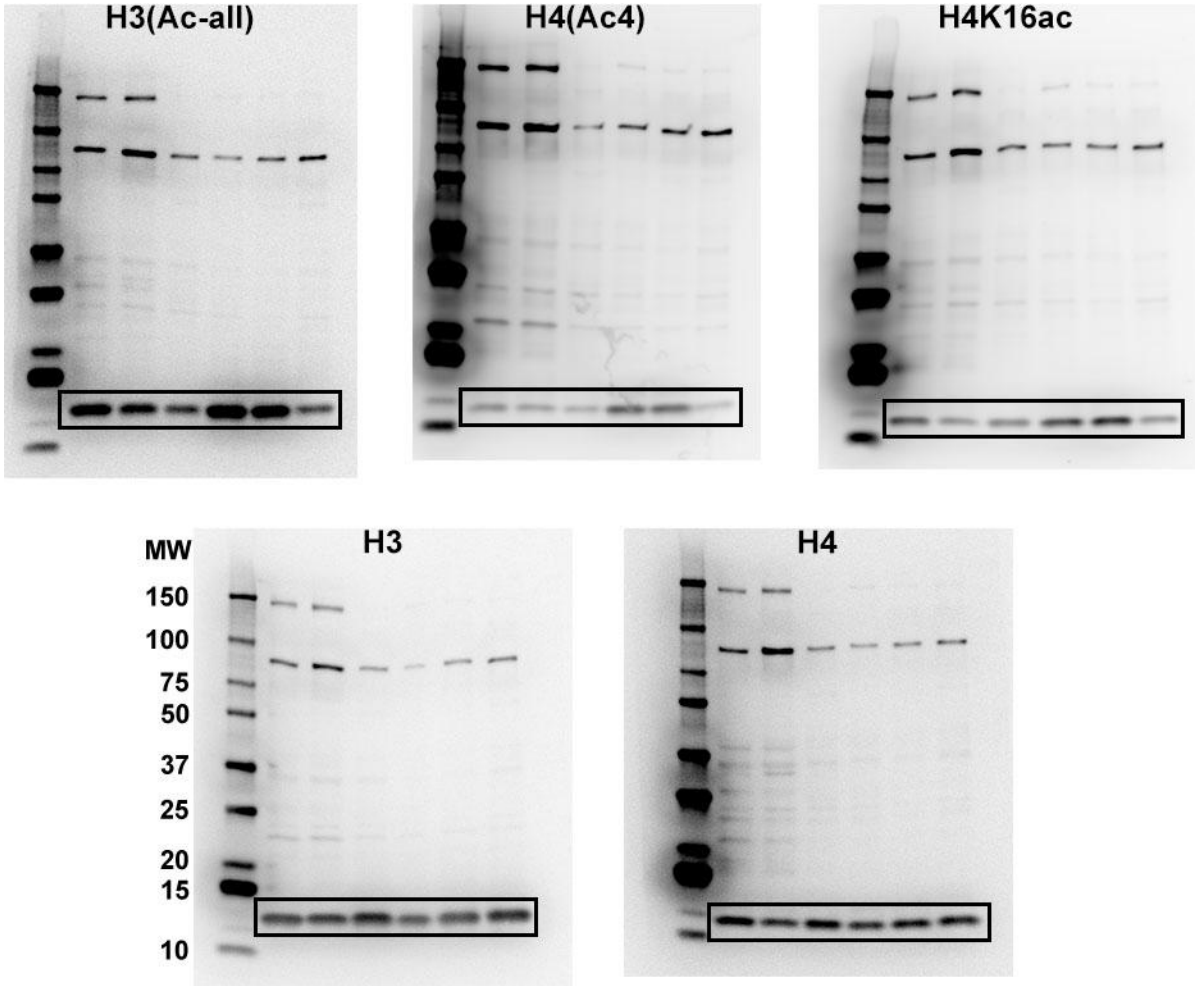

Figure S7. Uncropped immunoblots. For each immunoblot, the cropped bands are boxed at the bottom. The same molecular weight markers (MW, kilodaltons) were used for all 5 blots. Molecular weights are indicated to the left of the anti-H3 blot. The detected high-molecular weight proteins (> 75 kilodaltons) are non-specifically bound by the StrepTactin-HRP conjugate.

Table S1. Antibodies used.

Antigen	Primary antibody	Secondary antibody	Dilution	
			primary	secondary
Immunoblots				
H3 C-terminus	ab1791 (Abcam)	7074S (CST)	1:1000	1:5000
H4 C-terminus	ab10158 (Abcam)	7074S (CST)	1:1000	1:5000
Acetyl-H3	06-599 (Merck)	7074S (CST)	1:1000	1:5000
Acetyl-H4	06-866 (Merck)	7074S (CST)	1:1000	1:5000
H4K16ac	ab109463 (Abcam)	7074S (CST)	1:1000	1:5000
Immunofluorescence				
Acetyl-H3	06-599 (Merck)	A11008 (Thermo)	1:500	1:500
Acetyl-H4	06-866 (Merck)	A11008 (Thermo)	1:500	1:500
H4K16ac	ab109463 (Abcam)	A11008 (Thermo)	1:100	1:500
Pol II-CTD	ab210527 (Abcam) *	A11008 (Thermo)	1:1000	1:2000
Pol II-CTD-S2P	ab5095 (Abcam)	A11008 (Thermo)	1:1000	1:2000
Fibrillarin	NB300-269 (Novus)	A11001 (Thermo)	1:1000	1:2000

* This antibody is discontinued. CST = Cell Signaling Technology; Thermo = Thermo Fisher Scientific.

Table S2. Cryo-EM imaging and analysis details.

EM grids	CF200-Cu-50
Cryomicrotome feed	70 or 100 nm
Microscope	Titan Krios
Energy	300 keV
Camera: recording mode	Falcon II: integration
Tomography software	FEI Tomo4
Calibrated pixel sizes, unbinned	4.6 Å, 5.8 Å, 7.3 Å
Defocus (nominal, Defocus contrast)	−8 µm
Defocus (fitted, Defocus contrast)	−9 to −13 µm
Defocus (nominal, Volta contrast)	−0.5 or −1 µm
Cumulative dose	60 or 100 e^- / $Å^2$
Dose fractionation	1 / cosine
Tilt range: scheme	±60°: bidirectional
Tilt increment	2°
Tomogram processing & visualization	IMOD 4.9.12 and 4.10.22
Template matching	PEET 1.11 and 1.13.1
Subtomogram classification & averaging	RELION 2.1 and 3.0
Analysis scripts	https://github.com/anaphaze/ot-tools
Figure creation and editing; t-tests	Adobe Photoshop and Illustrator; Google sheets

Table S3. Cryotomogram details.

Tomogram ID	Sample	Figure / Analysis	Pixel size (Å)	Defocus † (µm)		DPC/ VPC
				nom	ref	
20170111_14	G1	S1C	7.3	10	9.8	DPC
20160212_00	G0	S1D	7.3	8	7.8	DPC
20160501_02	G1	2A,C *	4.6	1	n/d	VPC
20160711_01	G0	2B,D *	4.6	1	n/d	VPC
20160501_04	G1	3C,E,F / pack	4.6	1	n/d	VPC
20160711_20	G0	3D,G,H / pack	4.6	1	n/d	VPC
20190109_13	G0-20d	S5A,B	4.6	0.5	n/d	VPC
20181024_07	G0-20d	S5C	4.6	0.5	n/d	VPC
20181024_17	G0-20d	S5D	4.6	0.5	n/d	VPC
20160711_03	G0	5A,C / pack	4.6	1	n/d	VPC
20190103_23	TSA-G0	5B,D / pack	4.6	0.5	n/d	VPC
20160711_33	G0	pack	4.6	1	n/d	VPC
20160501_09	G1	pack	4.6	1	n/d	VPC
20160501_15	G1	pack	4.6	1	n/d	VPC
20160713_13	G1	pack	4.6	1	n/d	VPC
20181117_10	TSA-G0	pack	4.6	0.5	n/d	VPC
20190103_10	TSA-G0	pack	4.6	0.5	n/d	VPC
20190109_07	G0-20d	pack	4.6	0.5	n/d	VPC
20190123_07	G0-20d	pack	4.6	0.5	n/d	VPC
20190123_10	G0-20d	pack	4.6	0.5	n/d	VPC

G1 = G1 phase. G0 = G0 after a 24-hour incubation in EMM−N media. G0-20d = G0 after a 20-day incubation in EMM−N media. TSA-G0 = 24 hour incubation in EMM−N plus TSA. * The tomograms 20160501_02 and 20160711_01 have been deposited in EMDB as entry EMD-0875. † Nominal (nom) and refined (ref) defocus values; n/d = defocus refinement was not done for VPC data. DPC = defocus phase contrast; VPC = Volta phase contrast. Packing = Used for packing analysis attempts.